Real-Time Comparisons of VPR-Corrected Daily Rainfall Estimates with a Gauge Mesonet

ALDO BELLON, GYUWON LEE, ALAMELU KILAMBI, AND ISZTAR ZAWADZKI

J. S. Marshall Radar Observatory, Department of Atmospheric and Oceanic Sciences, McGill University, Montreal, Quebec, Canada

(Manuscript received 23 February 2006, in final form 11 October 2006)

ABSTRACT

The relative skill of two vertical-profile-of-reflectivity (VPR) correction techniques for daily accumulations on a selected dataset and a real-time dataset has been verified. The first technique (C_1) adjusts the 1-h rainfall amounts already derived on a Cartesian CAPPI map at an altitude of 1.5 km in a "one step" procedure using the range-dependent space–time-averaged VPR over the 1-h interval. The C_2 technique corrects the nonconvective polar reflectivity measurements of each 5-min radar cycle that are also centered at a height of 1.5 km according to a VPR that is similarly derived but over a shorter time interval. The results emphasize the importance of applying a VPR correction scheme—in particular, in a climatic regime in which most of the liquid precipitation falls from stratiform echoes. The crucial importance of the choice of datasets is also underlined, causing differences in the final assessment that may be greater than those between the various algorithms. Both techniques perform well with selected events of low bright band and thus with the greatest potential for improvement—in particular, when the bias is removed in a post facto analysis. However, when the VPR algorithm is tested in a real-time environment consisting of less strong or higher brightband situations and faces a variety of day-to-day precipitation, the improvement is substantially lower. RMS errors are reduced only from 61% to 48% in contrast with the reduction from 117% to 43% seen with the smaller sample of selected events. This is because other sources of error—in particular, the variability in the radar reflectivity–rainfall rate (Z–R) relationship—are often of the same magnitude as the VPR errors. An example is provided that shows how the bias from an improper Z–R relationship can reduce the true skill of a real-time VPR correction scheme.

1. Historical background

From the very early years of operational radar meteorology at McGill University, a basic product for a variety of applications has remained the CAPPI map, subsequently generated since the late 1960s from the available 24 elevation angles every 5 min. On account of the fairly extensive ground clutter of our S-band radar, which furthermore is located in the shallow valley of the St. Lawrence River with a high probability of anomalous propagation (AP), it was mandatory during those years of reflectivity-only data to center the CAPPI at a fairly high altitude: namely, at 10 000 ft (or ~3 km; Marshall and Ballantyne 1975). The advent of digital data by the mid-1970s allowed for the interpolation over the known regions of normal ground clutter, and thus permitted a lowering of the CAPPI to heights ranging from 1.5 to 2.5 km, depending on the season. Although the presence of the melting layer was well known, its impact was generally ignored or was considered to be unimportant because most of the emphasis was then on the detection and forecasting of severe convective weather (as implied by our initial name of Stormy Weather Group). However, when precipitation estimates were routinely transmitted to the local forecast office in the mid-1980s by the first version of our automatic radar processing system, flash-flood warnings were occasionally issued by the forecasters on the basis of accumulations generated from CAPPIs centered near the height of the brightband peak. A subsequent version of such a system, called the Radar Data Analysis, Processing, and Interactive Display (RAPID), enabled the forecasters at least to recognize properly such gross overestimations of surface rainfall. It provided a range-dependent vertical profile of reflectivity (VPR) with every CAPPI and accumulation map, with the VPR accompanying the latter being integrated

Corresponding author address: Dr. Aldo Bellon, J. S. Marshall Radar Observatory, McGill University, P.O. Box 198, Macdonald Campus, Ste-Anne de Bellevue, QC H9X 3V9, Canada.
E-mail: aldo.bellon@mcgill.ca

DOI: 10.1175/JAM2502.1

over the time interval of the accumulation. Our first attempt at actually providing VPR-corrected surface rainfall estimates was thus more readily achieved by adjusting the 1-h accumulations derived from CAPPI maps at heights of ~2 km (Bellon and Kilambi 1999).

The need to correct for the VPR had by then already been recognized by many researchers [Joss and Waldvogel (1990), Fabry et al. (1992), and Joss and Lee (1995), among others], and Koistinen (1991) actually implemented an operational VPR correction of daily rainfall estimates. Andrieu and Creutin (1995) deduced the mean VPR from the ratios of radar measurements at two elevation angles using an inverse method. Their technique was later extended by Vignal et al. (1999) to account for the local variability of the VPR by using radar data recorded at multiple elevation angles. Kitchen et al. (1994) have implemented a scheme to correct for the effects of bright band, range, and orographic growth by constructing an idealized reflectivity profile weighted by the radar-beam power at each pixel of the radar coverage. In addition to radar data from four elevation angles, surface temperature from synoptic observations and precipitation-top height inferred from infrared data were used to define the parameters of the space-varying VPR. Comparison with near-surface rain rates from a neighboring radar 40–120 km away on seven wet days characterized by a relatively low bright band resulted in the reduction of the rms error from ~110% to 55%. A subsequent attempt by Kitchen (1997) at improving the estimate of the reflectivity gradient above the bright band was only partially successful. Smyth and Illingworth (1998) have devised a simple method for identifying convection and have emphasized the importance of a separate correction for stratiform and convective precipitation. Mittermaier and Illingworth (2003) argue that, for the United Kingdom, operational model predictions of the freezing-level height used for fixing the height of the idealized vertical profile are better than that obtained from radar volumetric scans. Other algorithms, whether based on locally identified VPRs as implemented by Seo et al. (2000) or on the measured mean mesobeta profile within a 70-km range as outlined by Germann and Joss (2002), have eventually been verified with one or several days of surface "ground truth" as provided by rain gauges. Vignal et al. (2000) have compared their relative merit and concluded, on the basis of nine events and after a preliminary bias adjustment with one-half of the gauges, that the mean profile provides most of the reduction of the error from 44% to 25%, with the locally identified profiles further reducing the errors only slightly to 23%. A large-sample evaluation of the two basic methods has been carried out by Vignal and Krajewski (2001) using 2 yr of Weather Surveillance Radar-1988 Doppler (WSR-88D) data and the corresponding rain gauge observations from the Oklahoma Mesonet. A wide range of errors, from 200% to 10%, is obtained depending on range and the length of the accumulation (hourly, daily, or total). The outcome was similar to that in Vignal et al. (2000) and further concluded that the benefit of using locally derived VPRs diminishes with the length of the accumulation. A more considerable database of 8 yr has recently been analyzed by Germann et al. (2006) in their evaluation of the gradual improvement of precipitation measurements obtained over the difficult terrain of the Swiss Alps, after successive corrections for ground clutter and beam blocking as well as for VPR and bias effects. They consider the rainfall-weighted scatter of the radar:gauge ratios as a robust parameter for assessing the improved skill over the years. Dinku et al. (2002) also outline a procedure suitable for rainfall estimates over complex terrain. It is recognized that the results of such comparisons are not only dependent on the skill of the various VPR correction algorithms—that is, on their ability to take into account the actual space–time variability of the VPR—but also on the relative importance of the other well-known sources of radar–gauge (R–G) differences: namely, radar calibration, possible rain-path and wet radome attenuation (for C band), residual ground clutter and/or removal of precipitation by such a procedure, R–G temporal and spatial sampling differences, and the variability of the drop size distribution that affects the conversion of radar reflectivity into rainfall rate. A simulation study by Bellon et al. (2005) has attempted to isolate the expected improvement of a basic VPR correction technique resulting solely from the VPR as a function of brightband height, accumulation interval, averaging area, and uncertainties in the brightband height. By allowing for a realistic variability of the VPR, it was found that the latter limits the possible improvement by an amount greater than expected. Because the reviewers of that paper urged us also to evaluate our technique with actual surface measurements, the installation of a Mesonet during the summer of 2004 has permitted us to implement such a task in real time. In this paper, we thus report on all of the comparisons archived in real time of daily rainfall estimates continuously made over three study periods in the spring and autumn of 2005 and in the spring of 2006 to which were added eight rainfall events during the 2006 winter season. Details are provided in Table 1. The results from the regeneration of radar accumulation maps during the significant stratiform events from autumn 2004 (October–December), prior to the auto-

TABLE 1. Description of the data used in terms of the number of days in each test period, the number of R–G comparisons, and the average daily gauge rainfall (mm). This information is provided for a requirement of a daily rainfall of at least 2 mm, except for the last row for which 1 mm is considered.

Time period	Days	R–G pairs	G_{avg} (mm day^{-1})
Autumn 2004: 3 Oct–24 Dec	11	226	10.7
Spring 2005: 1 Apr–24 Jun	39	796	10.8
Autumn 2005: 8 Oct–30 Nov	19	503	13.2
Winter 2006: 15 Jan–15 Mar	8	250	12.2
Spring 2006: 8 Apr–3 Jun	27	575	8.4
Spring 2005, autumn 2005, winter 2006, and spring 2006	93	2124	10.9
As above but with threshold = 1 mm day^{-1}	98	2406	9.7

matic archival of the real-time comparisons, are also presented.

2. VPR correction methods with the McGill radar

During approximately the past 9 yr, as part of the McGill RAPID system, we have been constantly developing and updating various VPR correction schemes for the real-time surface radar rainfall estimates provided to the Montreal Weather Office. These maps are in the form of (240 × 240) arrays at both 1- and 2-km resolution, thus extending to 120 and 240 km from the radar, respectively. However, as already stated in the introduction, when constructing these Cartesian maps, the considerable ground clutter caused mainly by the sidelobes of our S-band radar prevents us from using any polar pixels from the 3D volume scan that are below ~1 km. We are thus forced, even at near ranges, to use data at an approximate height of 1.5 km, in a layer often affected by melting snow for a considerable part of our rainfall season. Nonetheless, the few echo-free pixels at the lower heights enable us to derive a reliable VPR that is then used for correcting the observations at the higher heights. The simulation of a nearer-range VPR is used to correct estimates made with the lowest elevation angle at farther ranges (>100 km). This lowest elevation may be in the snow if the bright band is low; otherwise, it would eventually traverse the bright band at some farther range. Currently, at every hour, four 1-h accumulations, denoted by C_0, C_1, C_2, and C_3, are generated by RAPID. However, the fourth method, the climatological C_3 algorithm, is not yet optimized for operational implementation and will thus be only briefly discussed without presenting its results.

a. VPR uncorrected (C_0)

Even though we refer to these estimates as "uncorrected" from the VPR point of view, their generation requires considerable processing of the raw data of the 24 elevation angles that are recorded at resolutions of 1° and 1 km up to 120 km (2 km between 120 and 240 km). This dataset, which is actually collected at a PRF of 600 or 1200 Hz, depending on the elevation angle, is first corrected for range and velocity folding. Then, because of the absence of a zero-velocity notch filter at the signal-processing level, pixels with normal and AP ground clutter are first identified at this resolution by means of an algorithm that computes the standard deviation of reflectivity from the seven 150-m gates before they are averaged into a 1-km bin. The 1 km × 1° pixel is then declared a ground echo if the standard deviation exceeds a threshold (3.3 dB) and if the absolute value of the mean radial velocity over the 1-km distance is less than 1.5 m s^{-1}. A technique similarly based on the characteristics of radar echoes proposed by Cho et al. (2006) is also being considered for our data. Precipitation information over the ground-echo pixels is then obtained by a range–azimuth constant-height interpolation of the neighboring "raining" pixels. However, ground echoes are simply removed and no interpolation is performed if the observed ground clutter area is more than 2 times the normal and greater than 3 times any precipitation detected. These criteria that imply severe AP or "AP only" conditions in the Montreal region prevent any residual weak ground echoes at the edge of the AP pattern to be spread over the entire AP region and ensure that ground-echo pixels are replaced only by precipitation information. After the polar-to-Cartesian transformation onto 1- and 2-km-resolution grid areas on a CAPPI map at a height of 1.5 km, the resultant maps, available every 5 min, are integrated over a desired time interval (typically 1 h) using an advection procedure that takes into account the propagation velocity of the precipitation area as illustrated in Fabry et al. (1994). Longer accumulations are simply obtained by summing the pregenerated 1-h accumulations.

b. Correction of 1-h accumulations (C_1)

Figure 1a shows an uncorrected 1-h accumulation map (C_0) generated from the CAPPIs centered at 2 km. The azimuthally averaged and time-integrated (1 h) range-dependent VPR usually shown on the bottom-right-hand corner of such maps is here presented separately as Fig. 1b. The integration is performed in reflectivity (Z) units. Five VPRs are in fact derived over 20-km range intervals from 10 to 110 km and at a vertical resolution of 0.2 km. Such a narrow vertical resolution may be appropriate for the lower altitudes because each 0.2-km slice is sufficiently sampled by the near-horizontal lower elevation angles but is unsuitable

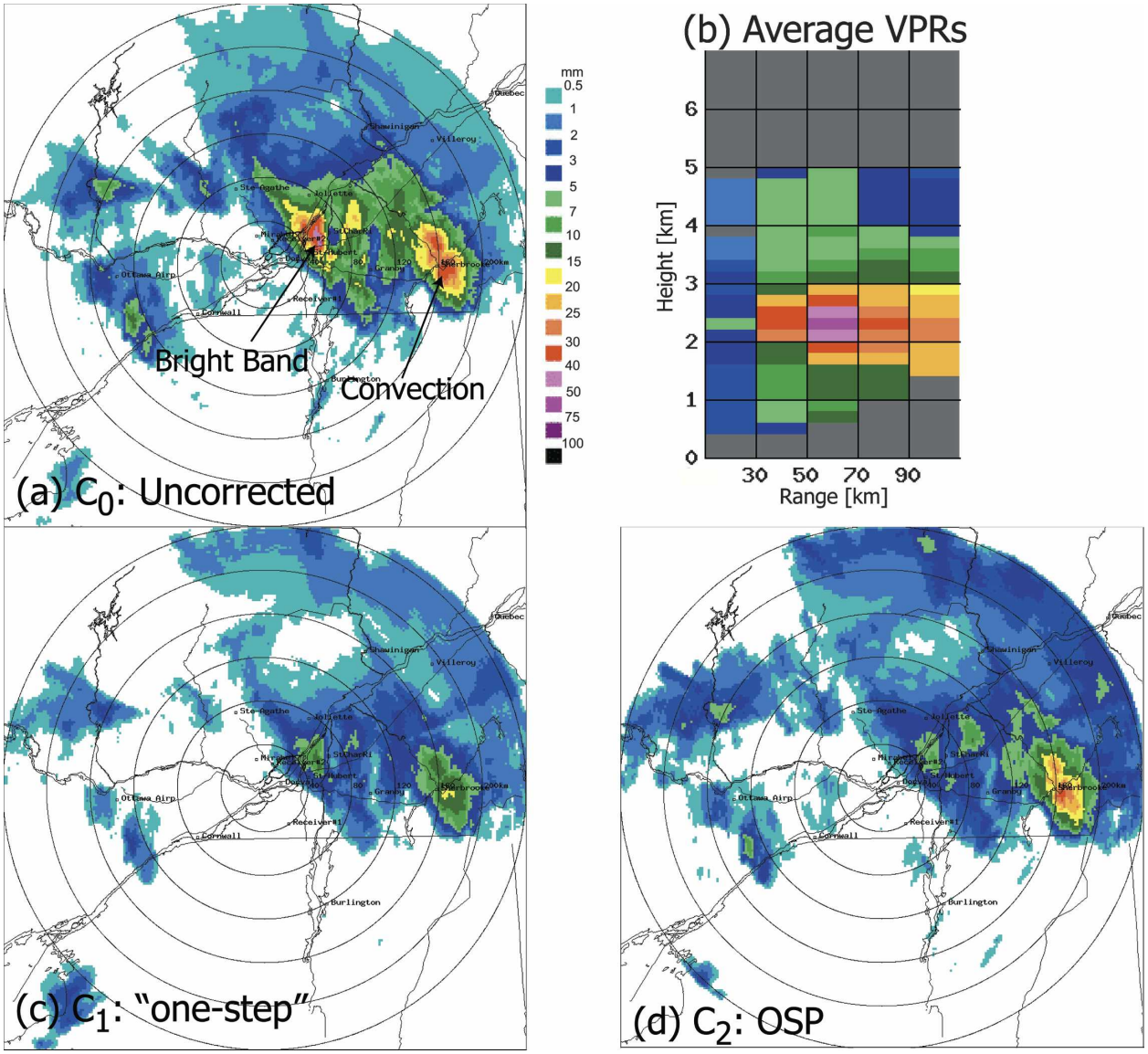

FIG. 1. (a) Uncorrected C_0 and (c) C_1 and (d) C_2 corrected 1-h accumulations showing the importance of recognizing convective pixels in a proper VPR correction scheme. In this example, C_0 is centered at a height of 2.0 km and C_2 is at ~1.3 km. Maps are at a resolution of 2 km with range rings 40 km apart, up to 240 km. (b) The time-integrated (1 h) range-dependent VPR display. Refer to the text for additional details.

for higher altitudes where fewer data points from a drastically reduced number of less-horizontal elevation angles can fall inside the upper slices. On the other hand, a large proportion of the data at the lower altitudes obtained by interpolation over the identified ground echoes, as described in section 2a, are thus not actually used in the derivation of the space–time VPR. A logarithmic vertical spacing would still have been more desirable, but the integration over a sufficiently large space–time domain avoids the shortcomings of a constant height resolution.

This VPR display would immediately warn the user of the unsuitability of a rainfall estimate derived from measurements at this height in representing surface precipitation. This is because, even though the nominal CAPPI height of 2 km is just below the height of the brightband peak, the finite number of elevation angles (24 in our case) causes the actual height of the data to be within a slice of ±200 m from the selected height. This oscillation will of course be larger for radar systems with fewer elevation angles. More important, this VPR exemplifies the variability of the VPR as a func-

tion of range, revealing the presence of a stronger bright band in the 50–70-km range associated mainly with the region pointed by an arrow in Fig. 1a. The widening vertical influence but with diminishing intensity of the bright band with range as sampled by a scanning radar with approximately a 1° beamwidth is also portrayed. The C_0 estimates are thus affected by the bright band over a much deeper layer, that is, over a greater range interval than would be deduced by assuming a typical brightband thickness of less than 0.5 km.

Our preliminary efforts, detailed in Bellon and Kilambi (1999), consisted of correcting in a simple one-step procedure the already-derived uncorrected 1-h accumulation on the basis of the reflectivity difference between the 2-km height and a suitably lower reference height of the VPR display. The lowest height is seen to be a function of range, but it is preferable to select the reference reflectivity to be at least 0.2 km higher to avoid any possible contamination by residual ground echoes. It is important to note that, even though the VPR shown seems to indicate that our accumulation maps should be based on low-angle PPIs rather than on higher CAPPIs, the VPR at the lower heights, as stated earlier, is based on the relatively few pixels with significant radial velocity (>1.5 m s^{-1}) located at least one polar pixel away from any possible ground echo. The latter is the union of an averaged ground echo mask (>0 dBZ) with a dynamic mask computed at every radar cycle. Our aim is to avoid any possible ground-echo contamination into the derived VPRs. For example, only ~35% of the pixels that fall inside the 0.8–1.0-km layer of the 30–50-km range are used to derive the VPR and <10% fall in the 0.6–0.8-km slice of the 10–30-km range interval. However, as mentioned at the beginning of this section, on account of geometrical considerations, which are further enhanced by the fact that our lower elevation angles are spaced much closer together than the upper angles, a greater number of reflectivity measurements can be integrated inside a 0.2-km layer at lower altitudes than at higher altitudes. The result is that the number of echo-free points actually used for averaging the reflectivity inside a 0.2-km layer at lower altitudes is comparable to that at middle altitudes (~3 km) and is actually larger than the number of points inside higher slices. The five correction factors (dBZ) obtained for each of the computed VPRs are converted into rainfall-rate factors and are interpolated in range at every kilometer. This technique presupposes that the reference height is not affected by the lower portion of the bright band. To reduce this possibility, we have opted to use only the first four VPRs. Because the 2-km-resolution maps extend up to a range of 240 km, it is desirable to estimate the appearance of the fourth VPR in the 70–90-km interval at successive ranges up to 240 km using a Gaussian simulation technique outlined in the appendix of Bellon et al. (2005) and illustrated in Fig. 3 of that paper. The proper correction factor for a given far range is thus obtained from the difference between the reflectivity of the Gaussian simulated profile at the true height of that range and the reflectivity at the reference height on the observed fourth VPR. If it is known that the reference height is indeed contaminated by the melting layer, the reference reflectivity is taken at a height of the brightband top. The recognition of this situation is aided by the information about the 0°C height from model output. We use the Rapid Update Cycle (RUC) forecasts (that were available online at http://maps.fsl.noaa.gov/), but it can also be deduced from the height of the peak reflectivity when the profile has been identified as that of a bright band. The brightband top can then be determined from the observed VPR as where the second derivative or curvature in the reflectivity drop above the brightband peak exceeds a threshold (~0.8 dBZ 200 m^{-1} 200 m^{-1}) or where a large drop in reflectivity across a 200-m layer in that region is followed by a much smaller drop over the next two layers. Otherwise, the brightband top is assumed to be a function of the peak reflectivity and range. When no bright band has been identified, it is assumed to be one-half of a beamwidth above the height of the 0°C isotherm as provided by the RUC model.

Figure 1c illustrates the results of the C_1 correction on the uncorrected C_0 1-h rainfall accumulation map of Fig. 1a. It is seen that the overestimation of the 1-h rainfalls as indicated by the VPR display has been reduced. However, in this one-step approach, the maximum east of the radar at a range of 160 km, which (according to tests later described in section 2c as well as from the visual examination of vertical cross sections) is mainly due to convective rainfall, has also been reduced. Thus, to remedy this problem, it is desirable to introduce a procedure that does not correct the convective regions of each of the 12 maps of our 5-min radar cycles within the 1-h interval.

c. Optimum surface precipitation (OSP, or C_2)

Although method C_1 is relatively simple for entirely stratiform systems, being readily applicable for Cartesian accumulation maps already generated at historically higher altitudes (~2 km), it has another disadvantage in that all rainfall amounts are corrected using their corresponding single 1-h VPR, regardless of whether the rain fell at the beginning or at the end of the accumulation interval. Moreover, after completing

the accumulation process, useful information regarding the stratiform or convective nature of the precipitation is lost. We are aware, as pointed out by Smyth and Illingworth (1998), that the vertical profiles of stratiform and convective precipitation differ significantly and therefore one should not use the same VPR for both precipitation types. This argument can be extended to include any other type of difference in VPRs, whether due to drizzle or to a change in the height or characteristics of the bright band. During our real-time tests, we have actually omitted the convective pixels during the generation of the VPR and then have chosen not to modify them during the correction procedure, although we envisage a possible increase of ~2 dBZ km^{-1} for heights above the 0°C isotherm as proposed by Smyth and Illingworth (1998). We identify convective pixels according to a simple test they have suggested that we have slightly modified to the requirement of a reflectivity of 32 dBZ at 2 km above the brightband peak. To ensure that no convective pixels are missed, an upper-level vertically integrated liquid (UVIL) map (Greene and Clark 1972) is generated by integrating $Z^{4/7}$ from a height of 4 km to echo top. A pixel that may have gone undetected according to the previous test is declared as such if the UVIL value exceeds a threshold of 1 kg m^{-2}. Therefore, an OSP algorithm, referred to here as method C_2, has been devised that seeks to correct every nonconvective polar pixel of each of the 12 "pseudo CAPPIs" needed for a 1-h accumulation. On account of the improved ground-echo identification, removal, and subsequent interpolation technique, we can afford to lower the altitude for the pseudo-CAPPI maps to a nominal height of ~1.5 km. The actual height variation is from 1.3 to 1.6 km within a range of ~100 km, sloping up to 2 km at a range of 125 km according to the first elevation angle of 0.5° (at 1200 PRF). The second elevation angle at 0.6° and 600 PRF is then used for farther ranges up to 240 km.

At every radar cycle, a VPR with similar spatial characteristics as the one shown with Fig. 1b is derived but is integrated over a user-selectable time interval that is shorter than 1 h (typically 30–45 min). Because of this shorter integration period, the reference reflectivity is actually obtained by averaging over an additional higher layer than that used for C_1. Unlike the method proposed by Germann and Joss (2002), the data from the required 5-min volume scans inside this interval are equally weighted. The nonconvective pixels of the pseudo CAPPI are corrected in a fashion as described for method C_1. To avoid improper corrections based on insufficient data, the VPR at the corresponding 20-km range interval must have a vertical extent of at least 2 km; otherwise, the VPR with the greatest vertical depth computed for the other range intervals is used. When none are available, a correction is not attempted. When extending the VPR correction to far ranges, it is very crucial to apply any positive correction to only the nonconvective portions of a precipitation system—that is, snow; otherwise, huge overestimations would result from embedded convection that requires little or no correction. In the converse situation, the inability to recognize a reflectivity as convective at closer range at a height within the brightband influence would cause an underestimation of the precipitation if this reflectivity is reduced. These are the primary reasons for separating convective and stratiform pixels in our C_2 procedure. The application of different Z–R relationships (where R is rainfall rate)—$Z = 200R^{1.5}$ for stratiform, from Lee and Zawadzki (2005), and $Z = 300R^{1.4}$ for convection—is of secondary importance and cannot be assessed with our dataset, which consists mainly of stratiform precipitation.

As illustrated in Fig. 1d, this C_2 method correctly recognizes the precipitation 160 km east of the radar as convective and thus, unlike C_1, maintains most of the associated higher rainfall estimates. We admit that the results shown later, being based on comparison with gauges at relatively close distances from the radar (<120 km), cannot ascertain to what extent this particular aspect of our procedure is successful at longer ranges. A delicate balance needs to be achieved between the urgency to reduce the excessive estimates of rainfall from brightband reflectivities and the necessity to maintain the strong rainfalls from convective cells at all ranges. In our ongoing modification of the algorithm, the limitation of any positive correction to only reflectivities below 35 dBZ, which are thus not likely to be convective, appears to be a way of ensuring both goals while avoiding gross overestimations from undetected convective cells at very far ranges.

The recognition of a low bright band affecting the reference range is used with C_2 in a manner similar to that of C_1, as is the procedure for estimating the correction for ranges beyond the fourth VPR. However, with C_2, if the reference range of one of the four range-dependent VPRs is contaminated by a low bright band because of beamwidth effects, a nearer noncontaminated VPR is used if available. The uncertainty associated with estimating the brightband top renders the subsequent estimates of surface rainfall that used it as the reference more prone to errors as well as to a greater time and space variability of such errors. The resulting discontinuity has been noticed on a few occasions by forecasters animating the corrected images. Other discontinuities are observed when maps that

have gone uncorrected because of a lack of a VPR suddenly are being corrected when sufficient precipitation comes within range and satisfies the minimum vertical extent of 2 km for the VPR. Different correction factors derived from the four range-dependent VPRs have also been seen to introduce artificial concentric patterns in short-term accumulation (<1 h). In general, these artifacts are less pronounced on longer accumulations.

Because C_2 "operates" on instantaneous reflectivity maps and not on 1-h rainfall accumulations as is the case with C_1, some additional refinements have been incorporated. 1) The C_2 can identify a VPR as low-level growth when a reflectivity maximum is observed near or at the reference height but far away from a higher 0°C isotherm height. The latter information is needed so as not to misinterpret the top portion of a very low bright band as low-level growth. In addition to the correction determined from the VPR, the identification of low-level growth permits an extra increase of up to 3 dBZ (depending on the observed vertical gradient just above the reference height) to account for the reflectivity growth between the reference height and the actual surface. 2) An attempt has also been made to identify evaporation when weak reflectivity aloft is observed with no reflectivity in the lowest two layers of the VPR. In this situation, the reflectivity at the pseudo-CAPPI height is decreased by as much as 5 dBZ if it is less than 20 dBZ. From our experience, evaporation can be detected during the approaching phase of an extensive low pressure system, particularly in winter, with echoes clearly only aloft. It is not as successful with scattered, small-scale cells in the dry air mass in the departing phase of a frontal system, mainly because the observed VPR is of insufficient depth to risk a correction. Therefore, we must state that the skill of these two refinements to the C_2 technique cannot be properly assessed by our experiment because we expect their importance to be relatively minor in our regions. 3) The C_2 method provides one obvious improvement that can be noticed in the northwest quadrant of Fig. 1d beyond ~90 km, which is severely affected by beam blocking of lower elevation angles by nearby hills. This improvement is simply achieved by selecting higher unblocked elevation angles in the generation of the OSP CAPPI map for the sector so affected between 300° and 335° azimuth. In so doing, the measurements are more likely to be influenced by the bright band, but the subsequent correction readily compensates for it. The higher elevations, however, do diminish the maximum useful range of such corrections.

We point out that we have applied both the C_1 and C_2 algorithms with some success in pure snowfall situations, generally yielding higher amounts than what would have been observed on the uncorrected pseudo-CAPPI height. However, before attempting a quantitative evaluation, a more robust algorithm that combines the derived VPR with the observed or model forecast vertical temperature structure is needed to infer hydrometeor type and size and thus to be able to correlate more truly the reflectivity aloft with surface snowfall rates.

d. Climatological correction (C_3)

We had originally intended also to verify the relative skill of a procedure that does not require the availability of observed VPRs within a certain range (90 km in our case), one capable of providing correction factors based on climatological profiles that can especially be used during the incoming phase of a precipitation system. This attempt has been reported in the simulation tests of Bellon et al. (2005). We had pointed out that the narrow range of possible reflectivity at heights of more than 2 km above the brightband peak, as compared with the broader spectrum of reflectivities at the surface, implied that a small error in selecting the most suitable curve in the snow would entail a significant error in the determination of the surface reflectivity. Smyth and Illingworth (1998) had also discussed this particular problem and underlined the large standard deviation of such average profiles, which precludes them from being used for surface rainfall estimates. Moreover, climatological profiles stratified by surface reflectivity do not reflect the observer's point of view of estimating the surface reflectivity from an observation aloft. We have recently derived climatological profiles stratified by the observed reflectivity at various heights above the brightband peak that show a similar narrowing of the dynamical range of the possible reflectivity below the bright band in the rain and near the surface. Because profiles derived in this fashion would have been more suitable for estimating surface reflectivity, we prefer to omit here the results obtained with those stratified by the surface reflectivity, even though an improvement relative to C_0 was generally achieved and C_3 was in fact similar to C_1 and C_2 for the spring-2006 test period.

3. Experimental setup

The McGill RAPID system provides maps of various radar-related parameters as specified on a menu by the user. In particular, accumulation maps over any time interval can be requested at a flexible frequency, but it is customary to generate 1-h accumulations every 5 min and longer accumulations (6, 12, and 24 h) every hour.

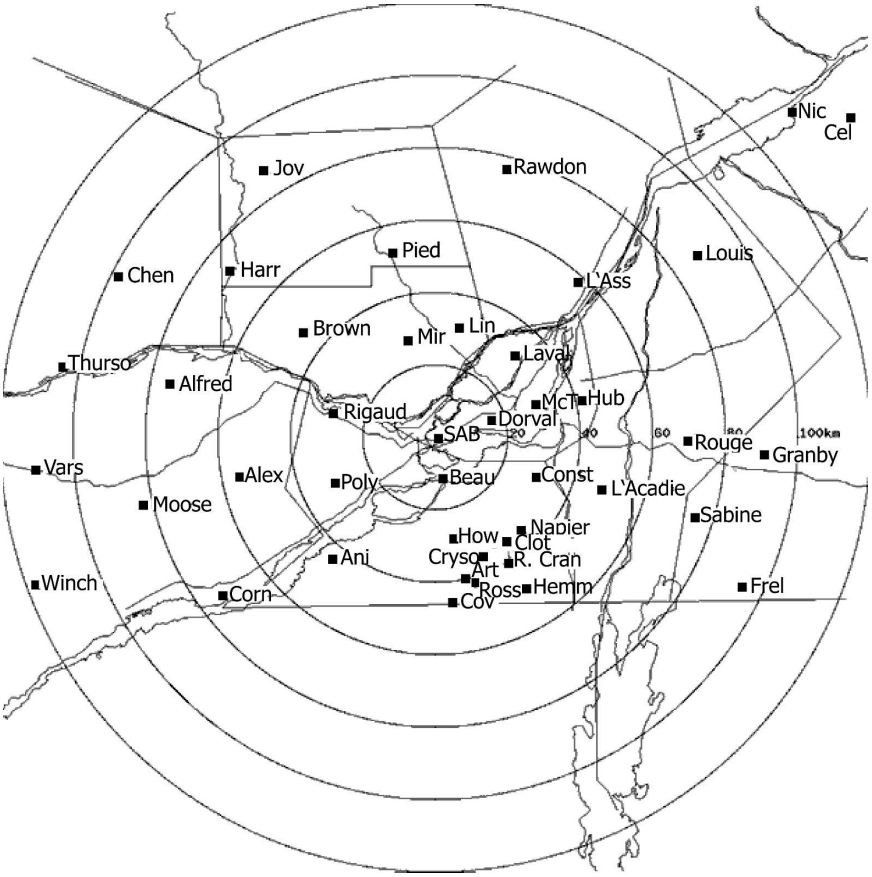

FIG. 2. Locations of the mesonet gauges within the McGill University radar coverage. Range rings are 20 km apart to a maximum west–east range of 120 km.

Each of these accumulations is in turn derived according to the methods described in section 2. Until 2004, these various options for the surface precipitation product were not verified except on the basis of some subjective visual assessment and acceptance by the forecasters on duty (and by the algorithm developers). The installation beginning in the spring of 2004 of a mesonet with gauges reporting rainfall in real time has finally provided the stimulus for comparing the relative skill of the VPR correction methods used. From 20 to 25 gauges were operational by midsummer until spring of 2005 at which time the total was increased to ~40 as shown in Fig. 2. All except one in the west-northwest at 140 km are located inside the typical (240 × 240) 1-km-resolution map centered over the McGill radar. As a consequence, at most five or six gauges could be considered at a sufficiently long range to evaluate the procedure for the Gaussian simulation of the farthest VPR, and none are at ranges enabling a verification of measurements made far up in the snow except in very low brightband situations. In this article, we are thus essentially evaluating the skill of the four observed VPRs within 90 km, as used by the C_1 and C_2 methods. They may be called "local" VPRs as done by Vignal et al. (1999), but in a strictly one-dimensional, that is, range-dependent, way. During our experiment, the height of the C_0 and C_1 CAPPIs has been lowered to 1.5 km, nearly coinciding with that for C_2. The main improvement expected from C_2 is thus from the application of the VPR correction at every radar cycle (5 min) rather than once per hour. Although the distinction of convective and stratiform precipitation is important, the test periods did not include sufficient convection for its evaluation. Likewise, the special treatment for the infrequent situations of evaporation and of low-level growth could not be evaluated.

Although the measurements from the mesonet can be retrieved at an hourly frequency, we have chosen for the moment to acquire the hourly totals for the previous day at only one appropriate time after midnight, to compute the 24-h precipitation totals for the previous day, and to compare them with the corresponding radar estimates. As discussed in greater detail during the presentation of the results in section 4a, a combination of

TABLE 2. Summary of the average verification scores for the various test periods described in Table 1. They are 1) bias B as the radar-to-gauge ratio, 2) AD, 3) RMS, and 4) cross-correlation coefficient r. The AD and RMS are normalized by the average daily rainfall and are expressed as a percentage. The three scores for the C_0, C_1, and C_2 methods, respectively, are provided for each parameter. These statistics have been derived for a requirement of a daily gauge rainfall $G \geq 2$ mm except for the last row for which a threshold of 1 mm is considered. The combined results from the four real-time test periods are shown in boldface.

Test period	B (R/G)	AD	RMS	r
Autumn 2004	1.33, 0.91, 0.99	51.1, 34.9, 30.5	117, 48.6, 42.7	0.52, 0.72, 0.76
Spring 2005	1.02, 0.85, 0.92	37.3, 35.9, 31.6	55.9, 53.2, 47.4	0.76, 0.79, 0.83
Autumn 2005	0.96, 0.83, 0.89	37.3, 33.2, 31.9	56.0, 46.6, 44.5	0.66, 0.78, 0.78
Winter 2006	1.13, 0.86, 0.89	35.4, 31.5, 29.6	50.5, 48.5, 45.9	0.84, 0.84, 0.85
Spring 2006	1.38, 1.07, 1.14	56.0, 36.8, 38.4	84.1, 54.0, 55.4	0.81, 0.87, 0.87
Spring 2005–06	**1.09, 0.89, 0.95**	**41.0, 34.7, 32.8**	**61.3, 51.2, 48.2**	**0.75, 0.81, 0.82**
Spring 2005–06 for $G \geq 1$ mm	1.11, 0.90, 0.97	42.2, 35.7, 34.0	65.3, 54.5, 51.4	0.77, 0.82, 0.84

R–G spatial and temporal sampling differences, Z–R uncertainties, and some quantization effects at the hourly scale was expected not only to yield large percentage errors, as reported by Vignal and Krajewski (2001), but also to mask part of the improvement possible with the correction methods. Working with 24-h accumulations also simplifies the process of visually detecting major discrepancies between the radar and gauge estimates that could be easily traced to an incomplete removal of AP echoes, strong rainfall gradients, or faulty gauges. During the "shakedown" period in the summer of 2004, these comparisons were obtained by user interaction with the RAPID system. Clicking on the 24-h accumulation map produced at midnight, or on a shorter one from the previous day, would result in a graphic depiction of the R–G comparisons. The interactive facility has been maintained, but the process of comparing daily accumulations at 0000 UTC became automated by early autumn; however, the resulting plots and corresponding R–G values were not archived until late March of 2005.

The availability of archived comparisons facilitates the summary of the results and allows a quick reanalysis for different radar and/or gauge rainfall thresholds as well as for the omission of R–G pairs for reasons similar to those outlined above but not evident in real time or shortly thereafter. For example, the requirement of a 24-h rainfall of at least 2 mm on the gauge automatically rejected the few cases of AP and other instances of faulty gauges that failed to report obvious rainfall amounts according to the 24-h radar accumulation. It also eliminated situations of radar overestimations of light rainfalls under conditions of evaporation or resulting from biological targets during the spring and autumn migration periods. Thus, less than 10 R–G pairs have been manually excluded from the real-time dataset of 98 days, mostly because of faulty gauges during part of the 24-h period. However, we have chosen not to adjust the radar estimates for a mean field bias, because part of our goal is to assess the accuracy of real-time VPR-corrected rainfall estimates, not those computed from a post facto analysis. Errors associated with fluctuations in the radar calibration and, especially, with the variability of the Z–R relationship are thus compounded with those resulting from the VPR. By contrast, radar estimates for the major rainfall events from October to December of 2004 have been regenerated from the archived raw volume scans using the RAPID simulation facility by taking into account some known calibration variation and by adjusting for a more suitable Z–R relationship. In this effort, we have implemented a procedure outlined by Lee and Zawadzki (2005, 2006) that incorporates data from a disdrometer nearly collocated with the radar site. We have selected 11 days, all extensive and deep stratiform systems, with the 6 days after mid-November characterized by a low and intense bright band. The real-time datasets instead include a variety of precipitation systems; still, they are mainly stratiform with the bright band at various heights, but also some are convective and/or cellular, with some instances of evaporation and with a large range in daily rainfall amounts.

4. Results

a. Verification statistics

We use the well-known statistics of bias B (radar-to-gauge ratio), correlation coefficient r, mean absolute difference (AD), and root-mean-square error (RMS), with the latter two normalized by the average gauge rainfall and expressed as a percentage to verify the skill of the various methods tested for each dataset. The three values given under their respective columns of Table 2 refer to the C_0, C_1, and C_2 methods, respectively. The choice of a rainfall threshold affects the magnitude of the results as well as whether it is required that such threshold be exceeded by only the gauge measurement or by either the gauge *or* the radar

estimate. We have opted to present the results in Table 2 mainly for a requirement of 2 mm on only the gauge to concentrate on significant rainfalls and to eliminate unwanted comparisons, as discussed in the previous section. Tests with thresholds from 0.1 to 5.0 mm yielded the expected changes in the error statistics, mainly because of their effect on the corresponding average rainfall. The results for a threshold of 1 mm have been added in the last row of Table 2. However, the relative skill of the VPR correction procedures remained essentially unaltered. The radar estimate selected for the comparison is the average of the nine (1 km $\times$ 1 km) Cartesian pixels centered on the gauge location. Results are only marginally affected by selecting the center pixel, whereas better scores are obviously obtained by seeking the best match in that neighborhood, with the latter choice being perhaps more meaningful for convective precipitation. However, because the relative skill of the various methods is again not influenced by these different approaches, they are not presented here. We also point out that we have not used the critical success index (CSI) parameter because, being defined as a ratio of hits and misses usually above a relatively low rainfall threshold, it is mainly used to evaluate the quality of the estimates in a "rain–no-rain" sense. Moreover we have found that it remains relatively insensitive to the methods tested even after increasing the threshold to 5 mm and more. The reason is that, whereas the CSI scores are obviously reduced for all methods, only the small percentage of R–G pairs lying near the boundary of the threshold are being compared, thus ignoring most of the other changes among the various methods taking place far above or below the threshold. The correlation coefficient r, which we have nonetheless chosen to include in Table 2, also does not effectively differentiate among the three methods tested, being unable to separate distinctly the C_1 and C_2 methods and providing relatively little improvement with the C_0 score except for the autumn-2004 events. The latter contained 11 selected cases of strong stratiform systems with a low bright band that have the most to benefit from a VPR correction—in particular, when the bias is removed in a post facto analysis. Therefore, Table 2 shows that the VPR correction schemes achieved a greater improvement than with any of the other real-time datasets that include all of the raining days over the indicated period and with the bias not known in real time. This result is the natural outcome of a systematic verification approach as recommended by Germann at al. (2006).

In general, C_2 yields the most error reduction in both the selected and real-time datasets, with the exception of the spring-2006 period, for which C_1 is marginally, but not statistically, better. The RMS is reduced from 117% to 43% for the autumn-2004 events and from 61% to 48% for the entire real-time dataset of over 90 days of precipitation. However, the limited sample of the autumn events, with only slightly over 200 comparisons, is susceptible to the strong influence of some key days. For example, excluding the very low brightband case of 21 November 2004, in which the VPR schemes performed very well, reducing uncorrected errors $O(400\%)$ to $\sim$60%, would drastically decrease the average RMS error for C_0 to 60% (from 117%). Because the average score for C_2 would be only slightly affected, being maintained at $\sim$40%, the gap between these schemes would be sharply decreased. The AD score is, of course, less sensitive to large R–G differences, yielding lower-magnitude errors, but the differences among the three estimates among the various test periods are similar in a relative sense. The improvement over the C_0 estimates is evident in all periods except for the fewer events in winter of 2006. However, the C_1 method, with all of its simplicity of operating on one accumulation map per hour rather than on 12 rain-rate maps, yields an improvement that is almost as good as that of C_2 for some real-time periods, possibly in part as a result of the fact that very little convection was encountered during the periods tested. The 2124 daily R–G comparisons as a whole yield RMS errors of 61%, 51%, and 48% for C_0, C_1, and C_2, respectively, and 41%, 35%, and 33% for the AD parameter.

This tendency for only a minor improvement derived from a technique with increased complexity has also been encountered by Vignal et al. (2000) who, from an uncorrected standard error of 44%, only obtained a slight reduction from 25% to 23% using the more complicated procedure of computing locally derived VPRs rather than the simpler mean VPR. These smaller percent errors for their daily estimates relative to those of our Table 2 are probably due to the bias adjustment that is made using half of the gauges prior the computation of the error on the remaining gauges. The results shown in Table 1 of Vignal and Krajewski (2001), where no such bias adjustment has been performed, are perhaps more readily comparable with our own. However, they choose to describe their results in terms of the percent reduction from the uncorrected errors, rather than as a percent of the average rainfall amount as we, and Vignal et al. (2000), have done. Thus, in our terminology, at ranges of 100–150 km where the bright band affects the uncorrected measurements during their experiment, uncorrected RMS error for daily accumulations of $\sim$100% is decreased to 80% with a mean VPR and again, only moderately less (to 70%) with locally identified VPRs. At closer ranges that are

mostly below the bright band, errors are confined within the 55%–75% interval, with, as expected, very little distinction between the corrected and uncorrected estimates. The corresponding errors for 1-h verifications, which attain magnitudes from 150% to over 200%, emphasize the R–G sampling problems that occur at shorter time scales that may mask the gain achieved by the correction. A similar conclusion can be reached from the results of Seo et al. (2000) whose VPR adjustment procedure achieves a 40% error reduction with storm totals on the order of 40 h, as compared with 10% for hourly verifications.

From an examination of the change in bias after correction, it appears, with the possible exception of the spring of 2006 and, of course, the autumn-2004 dataset for which a daily bias adjustment was applied, that our radar is slightly underestimating rainfall, causing a further underestimation whenever any of the VPR correction techniques was applied, resulting in a bias lower than 1.0. We show in section 4b that such combination tends to mask some of the improvement derived from the VPR correction techniques. The frequent occurrence of drizzle precipitation while using the default climatological Z–R and some uncertainties in radar calibration during certain periods of hardware modifications that were made to satisfy research and operational needs of our radar system may explain this underestimation, which is on the order of 1 dB or less. The consistent lower bias obtained with C_1 when compared with C_2 for all test periods is more difficult to explain. We are aware that the C_2 method reduces the bias to a lesser extent than C_1 because, as illustrated in Fig. 1, C_2 does not reduce the rainfall rates associated with convection, but the latter was infrequent in our test periods. The fact that C_2 incorporates some low-level growth, with the opposite effects of evaporation being minimal, may be another factor. However, considering that the differences in the biases between the two methods are not unduly large, we cannot honestly state with assured certainty that these are indeed the reasons or whether there may be other causes.

The scatterplots of the comparisons for the autumn events are presented in Fig. 3, and those for the entire real-time test are in Fig. 4. On account of the wide range of daily rainfall amounts during this period, a logarithmic scale is used. The better performance of the VPR correction methods is more evident in Fig. 3 and is less noticeable in Fig. 4, whereas the differences between C_1 and C_2 are undistinguishable. Some of the statistics reported in Table 2 have been provided with these scatterplots to better assess the skill of the correction procedures. However, the statistics in Table 2 as well as the scatterplots do not convey a proper picture of the situation, because we cannot infer from them whether the average improvement is the result of slightly better estimates for all R–G pairs or whether a larger improvement on some R–G pairs is reduced by some worse results on other pairs. Thus, for any two radar estimates according to methods m and n, we compute the relative difference D_i from the gauge value G_i as

$$D_i = (|R_{i,m} - G_i| - |R_{i,n} - G_i|). \quad (1)$$

It is obvious that $D_i > 0$ means that method n is closer to the gauge estimate than is method m, and vice versa for $D_i < 0$. Two cumulative distributions of D_i, in discrete units of 1 mm, are then obtained by summing the negative and positive occurrences separately. The integration is initiated from the largest absolute value of D_i and is terminated at $|D_i| = 1$ mm. The results for methods C_0 and C_2 are shown in Fig. 5a,b for the autumn-2004 and the entire real-time tests, respectively. Taking Fig. 5b as an example, the interpretation is as follows: of the 2124 R–G comparisons, there were 702 instances in which C_2 was closer to the gauge value than C_0 by at least 1 mm and 389 cases in which the opposite was true, the remaining 1033 cases with $D < 1.0$ mm not being plotted. In 206 cases, the improvement by C_2 with respect to C_0 was at least 5 mm, as compared with 45 occurrences in which the uncorrected estimate was better than the corrected estimate by that threshold. We should not be surprised at such results—in particular, in real-time experiments without a bias adjustment. (Note that in Fig. 5a there are no instances in which C_0 is better than C_2 by more than 8 mm, as compared with 19 such occurrences for C_2.) If the uncorrected radar estimates are already underestimating the rainfall because of an improper radar calibration or Z–R relationship, the VPR correction technique would further reduce the estimates that are considered to be affected by the bright band, causing a larger deviation from the gauge value. Even when such problems are not a factor, it must be realized that the correction factors obtained from the space–time-averaged VPR are *average* corrections, which tend to undercorrect the regions affected by a stronger bright band but also to overcorrect the weaker brightband regions. This comment falls into the wider discussion of the representativeness of the derived VPR in rapidly evolving conditions or when applied to regions over which it has not been derived. There is a possibility of making matters worse by applying an improper correction, as clearly illustrated by Fig. 5. Sampling differences between radar and gauges can also contribute to apparent worse results. Such occurrences may also be the result of incorrectly choosing the reference height in low-brightband situations. In

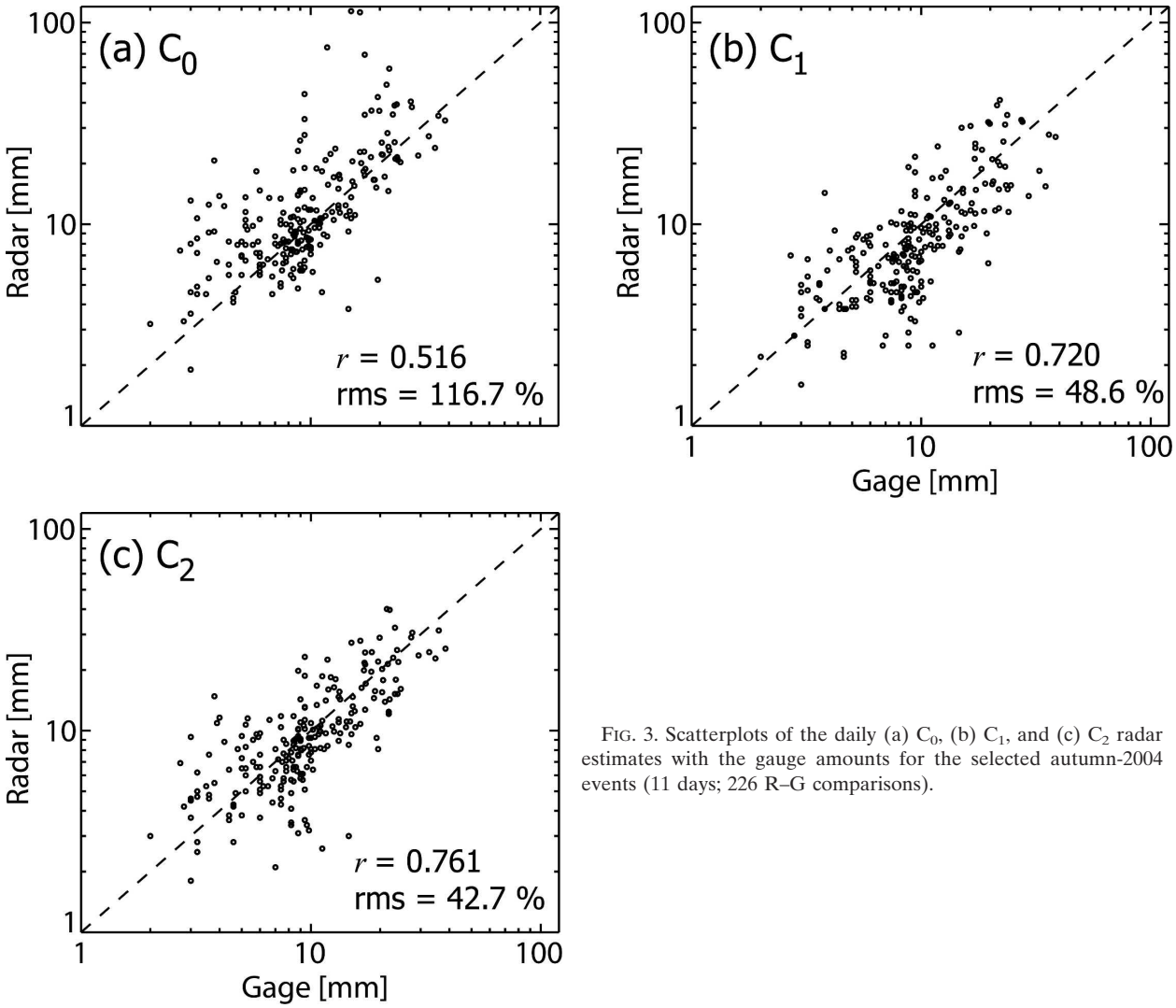

FIG. 3. Scatterplots of the daily (a) C_0, (b) C_1, and (c) C_2 radar estimates with the gauge amounts for the selected autumn-2004 events (11 days; 226 R–G comparisons).

such cases, the post facto analyses in which the actual 0°C height can be correctly provided have a definite advantage over real-time experiments in which such information is provided by NWP forecasts.

b. Z–R considerations

We have stated that, with the exception of the autumn-2004 dataset, all comparisons have been tabulated as computed in real time, without first correcting for the mean field bias for each day. As a consequence, the bias and error scores do not reflect the true skill of the methods tested because of the influence of other sources of error. For example, the overall uncorrected bias for the sets for spring and autumn of 2005 shown in Table 2 seems to indicate that a general underestimation of the rainfall has been rendered worse by the VPR correction schemes. The cause of the underestimation is not necessarily an improper radar calibration but could equally be an inappropriate *Z–R* relationship, the two sources of error being largely indistinguishable. The availability of a disdrometer in close proximity to the radar permits a verification of both its calibration status and a determination of the optimum *Z–R* relationship to be used on a given day (Lee and Zawadzki 2005). The case of 23 April 2005 in Fig. 6 illustrates well how an improper *Z–R* relationship can mask the improvement of a VPR correction scheme. The left-hand plots are the real-time comparisons obtained with the climatological $Z = 200R^{1.5}$ relationship, showing an apparent overestimation ($B = 1.18$) being reduced by C_2 to an underestimation ($B = 0.83$) while only marginally improving the RMS error from 44% to 40%. A disdrometer analysis later indicated that this day was characterized by drizzle precipitation necessitating a *Z–R*

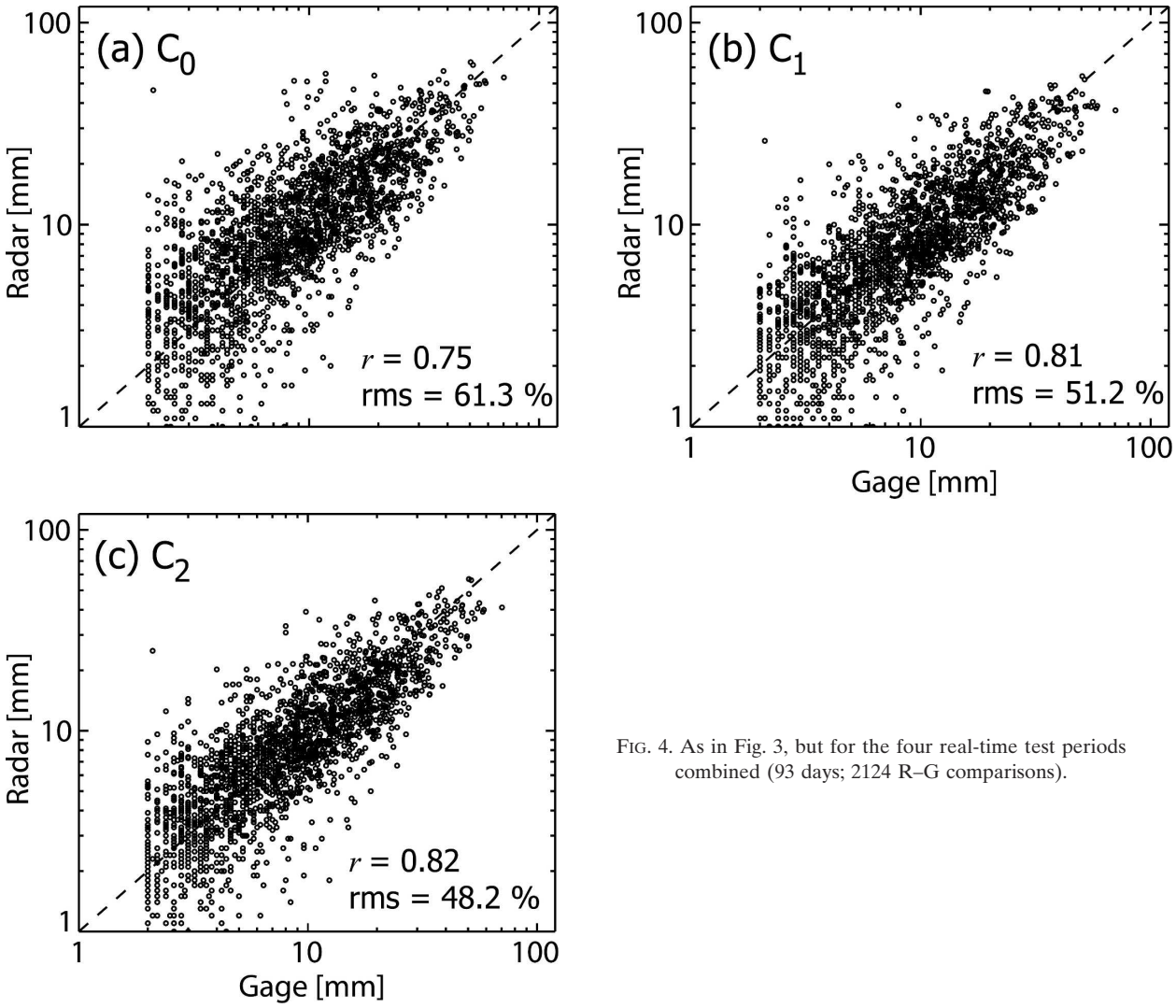

FIG. 4. As in Fig. 3, but for the four real-time test periods combined (93 days; 2124 R–G comparisons).

relationship on the order of $Z = 140R^{1.6}$. When the comparison is repeated after regenerating the radar estimates with the updated Z–R relationship, it is revealed that the true overestimation of over 40% is properly reduced to a mere 6% while the RMS error is decreased from 59% to 36%. A similar situation has been seen for a few other days (notably on 17 June 2005 and in mid-May 2006) on which again drizzle precipitation initially underestimated by the climatological Z–R relationship was furthered underestimated by the correction schemes. At other times, when an underestimation by C_0 is rendered worse by all of the VPR correction schemes, the need for a long, uninterrupted precipitation period for a robust disdrometer analysis prevents the reaching of a similar conclusion. Nonetheless, we can conclude that the true skill of a real-time VPR correction scheme cannot be fully realized unless the bias of the uncorrected estimates can be detected and removed in an operational environment. Attempting such a procedure in real time, whether using disdrometric data or with a dense network of rain gauges, represents an interesting challenge that will be the goal of our future research.

5. Conclusions

We have verified the relative skill of two VPR correction techniques for daily accumulations on both selected and real-time datasets. The first technique (C_1) adjusts 1-h rainfall amounts already derived on a 1.5-km CAPPI in a "one step" procedure using the range-dependent space–time-averaged VPR over the 1-h interval. The C_2 technique corrects the nonconvective pixels of the 5-min polar reflectivity measurements according to the VPR available at the time of each of the 12 scanning cycles, but averaged over a shorter time interval (~30–45 min). It partially takes into account

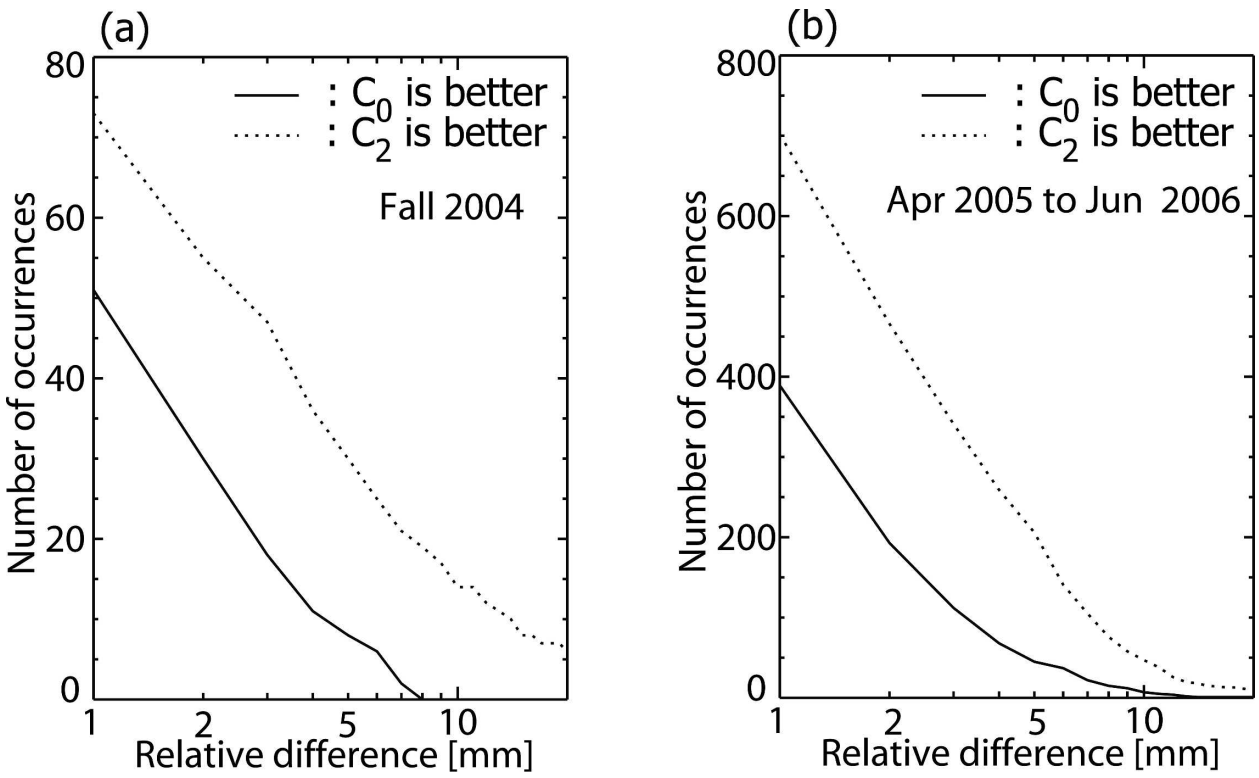

FIG. 5. Cumulative number of occurrences for which the C_0 (solid line) or the C_2 (dotted line) estimates were closer to the gauge value for (a) autumn 2004 and (b) the entire real-time test period. See text for examples of the proper interpretation of these curves.

evaporation, low-level growth, and beam blocking. It applies a different *Z–R* relationship for the convective and stratiform pixels, but the main advantage of this separation is that it prevents the positive correction of convective pixels that would yield gross overestimations at far range. This feature, however, cannot be assessed, because our test periods shown on Table 1 consist almost exclusively of stratiform precipitation and the rain gauge network is within 120 km from the radar. Unlike the post facto analysis of the autumn-2004 set, no adjustment for the mean field bias has been attempted with the real-time sets because we wanted to duplicate an operational environment in which such a procedure is still considered to be risky. The results in Table 2 emphasize the crucial importance of the choice of datasets, causing differences in the final assessment that may be greater than those among the various algorithms. Both correction techniques perform well with the autumn-2004 dataset, with C_2 displaying a noticeable advantage. This result is not surprising, considering that it included events with low bright bands and thus with the greatest potential for improvement—in particular, when the bias is removed in the post facto analysis. However, when the VPR algorithm was tested in a real-time environment consisting of less-strong or higher brightband situations and with a variety of day-to-day precipitation, the improvement is substantially lower and the differences between the C_1 and C_2 scores become marginal. The spring-2006 test period may be considered as an exception to the first part of this statement when uncorrected RMS errors of 84% of the average rainfall were reduced to ~55% with both methods. For the entire real-time test period, the C_2 method reduces the RMS errors from 61% to 48%, in contrast with the reduction from 117% to 43% seen with the autumn-2004 events. This is because other sources of error—in particular, the variability in the *Z–R* relationship and some uncertainties in radar calibration—are often of the same magnitude as the VPR errors. This has been demonstrated by the example in Fig. 6. Despite the greater complexity of C_2, it scored only slightly better than C_1, by further improving the AD and RMS statistics by merely 2% and 3%, respectively.

The results of an evaluation of any technique with selected cases should be accepted with caution if such a technique is meant for real-time operational applications. In our case, the need to precorrect for the mean field bias using an appropriate *Z–R* relationship is of utmost importance and, to a lesser extent, also important is the necessity to monitor the radar calibration.

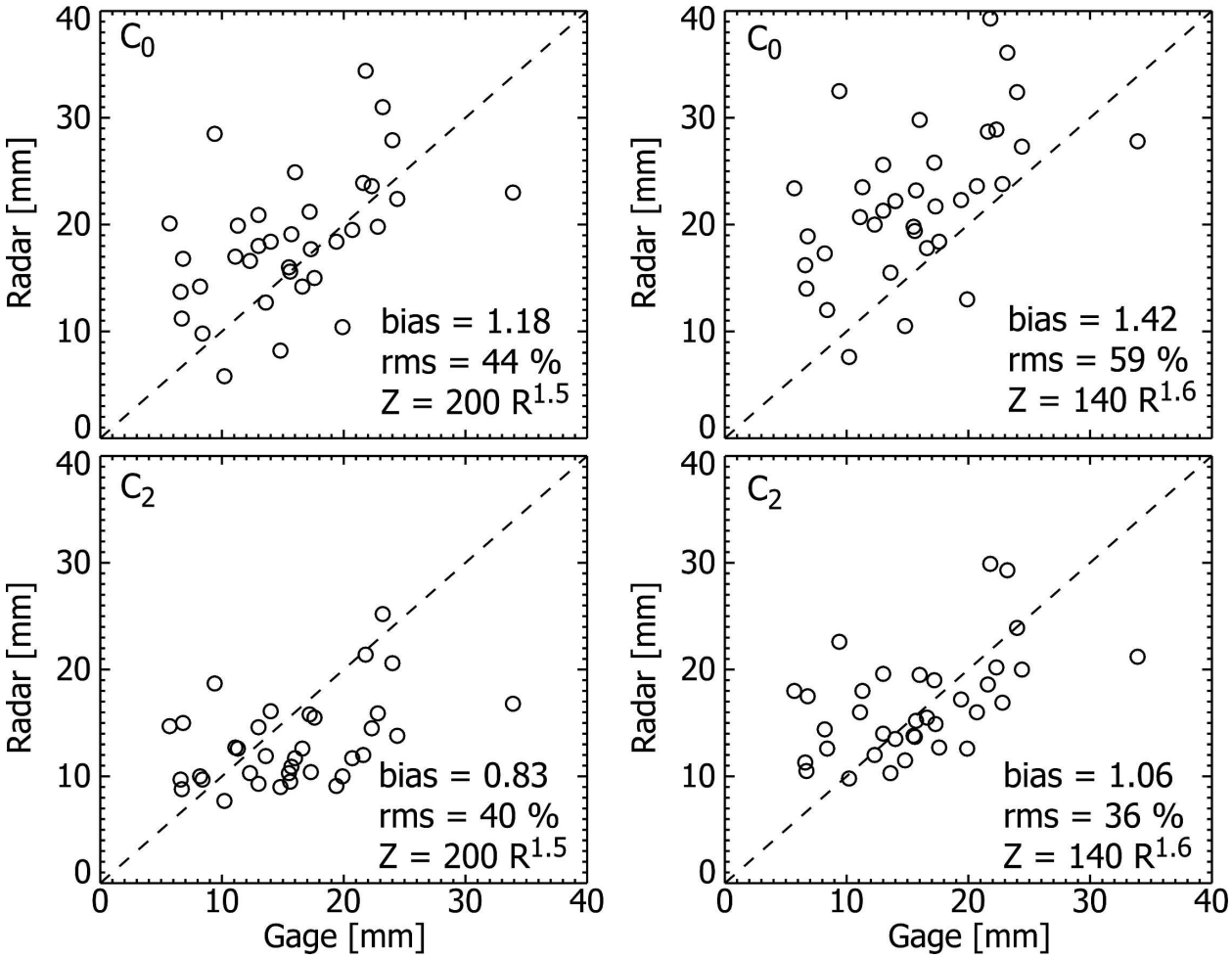

FIG. 6. Scatterplots for the (top) C_0 and (bottom) C_2 daily R–G comparisons on 23 Apr 2005 with the (left) climatological $Z = 200R^{1.5}$ relationship and the (right) disdrometer-derived $Z = 140R^{1.6}$ relationship showing how the bias from an improper Z–R can mask the true skill of a VPR correction scheme.

We hope to achieve this goal by applying emerging techniques of Lee and Zawadzki (2005a, 2006) that incorporate data from a disdrometer and a scanning radar. However, we remain aware of the limitations of disdrometric observations at a point when correcting radar measurements over an area within a radius of at least 120 km.

We conclude by pointing out that the correction of the vertical profile of reflectivity has some physical meanings. Since Waldvogel (1974) first reported the relationship among riming, the intensity of bright band, and the variation of drop size distributions, extensive research has been performed to reveal the physical meaning of the variation of the brightband intensity (Fabry and Zawadzki 1995; Huggel et al. 1996; Zawadzki et al. 2005). It demonstrates that the intensity and depth of the bright band are a good indication of snow growth above: riming produces a weak bright band whereas aggregation generates a thick and intense bright band. Thus, the VPR correction, especially local VPR correction, captures the variation of the intensity of the bright band resulting from the different microphysical processes.

Acknowledgments. This work was funded by a grant from the Canadian Foundation for Climate and Atmospheric Sciences.

REFERENCES

Andrieu, H., and J. D. Creutin, 1995: Identification of vertical profiles of radar reflectivity for hydrological applications using an inverse method. Part I: Formulation. *J. Appl. Meteor.,* **34,** 225–239.

Bellon, A., and A. Kilambi, 1999: Updates to the McGill RAPID system. Preprints, *29th Int. Conf. on Radar Meteorology,* Montreal, QC, Canada, Amer. Meteor. Soc., 121–124.

——, G. Lee, and I. Zawadzki, 2005: Error statistics of VPR corrections in stratiform precipitation. *J. Appl. Meteor.,* **44,** 998–1015.

Cho, Y. H., G. W. Lee, I. Zawadzki, and K.-E. Kim, 2006: Identification and removal of ground echoes and anomalous propagation using the characteristics of radar echoes. *J. Atmos. Oceanic Technol.,* **23,** 1206–1222.

Dinku, T., E. N. Anagnostou, and M. Borga, 2002: Improving radar-based estimation of rainfall over complex terrain. *J. Appl. Meteor.,* **41,** 1163–1178.

Fabry, F., and I. Zawadzki, 1995: Long term radar observations of the melting layer of precipitation and their interpretation. *J. Atmos. Sci.,* **52,** 838–851.

——, G. L. Austin, and D. Tees, 1992: The accuracy of rainfall estimates by radar as a function of range. *Quart. J. Roy. Meteor. Soc.,* **118,** 435–453.

——, A. Bellon, M. R. Duncan, and G. L. Austin, 1994: High resolution rainfall measurements by radar for very small basins: The sampling problem re-examined. *J. Hydrol.,* **161,** 415–428.

Germann, U., and J. Joss, 2002: Mesobeta profiles to extrapolate radar precipitation measurements above the Alps to the ground level. *J. Appl. Meteor.,* **41,** 542–557.

——, G. Galli, M. Boscacci, and M. Bolliger, 2006: Radar precipitation measurement in a mountainous region. *Quart. J. Roy. Meteor. Soc.,* **132,** 1669–1692.

Greene, D. R., and R. A. Clark, 1972: Vertically integrated liquid water content—A new analysis tool. *Mon. Wea. Rev.,* **100,** 548–552.

Huggel, A., W. Schmid, and A. Waldvogel, 1996: Raindrop size distributions and the radar bright band. *J. Appl. Meteor.,* **35,** 1688–1702.

Joss, J., and A. Waldvogel, 1990: Precipitation measurements and hydrology. *Radar in Meteorology,* D. Atlas, Ed., Amer. Meteor. Soc., 577–606.

——, and R. Lee, 1995: The application of radar–gauge comparisons to operational precipitation profile corrections. *J. Appl. Meteor.,* **34,** 2612–2630.

Kitchen, M., 1997: Towards improved radar estimates of surface precipitation at long range. *Quart. J. Roy. Meteor. Soc.,* **123,** 145–163.

——, R. Brown, and A. G. Davies, 1994: Real-time correction of weather radar data for the effects of bright band, range and orographic growth in widespread precipitation. *Quart. J. Roy. Meteor. Soc.,* **120,** 1231–1254.

Koistinen, J., 1991: Operational correction of radar rainfall errors due to the vertical reflectivity profile. Preprints, *25th Int. Conf. on Radar Meteorology,* Paris, France, Amer. Meteor. Soc., 91–94.

Lee, G. W., and I. Zawadzki, 2005: Variability of drop size distributions: Time scale dependence of the variability and its effects on rain estimation. *J. Appl. Meteor.,* **44,** 241–255.

——, and ——, 2006: Radar calibration by gage, disdrometer, and polarimetry: Theoretical limit caused by the variability of drop size distribution and application to fast scanning operational radar data. *J. Hydrol.,* **328,** 83–97.

Marshall, J. S., and E. H. Ballantyne, 1975: Weather surveillance radar. *J. Appl. Meteor.,* **14,** 1317–1338.

Mittermaier, M. P., and A. J. Illingworth, 2003: Comparison of model-derived and radar-observed freezing-level heights: Implications for vertical reflectivity profile-correction schemes. *Quart. J. Roy. Meteor. Soc.,* **129,** 83–95.

Seo, D.-J., J. Breidenbach, R. Fulton, D. Miller, and T. O'Bannon, 2000: Real-time adjustment of range-dependent biases in WSR-88D rainfall estimates due to nonuniform vertical profile of reflectivity. *J. Hydrometeor,* **1,** 222–240.

Smyth, T. J., and A. J. Illingworth, 1998: Radar estimates of rainfall rates at the ground in bright band and non-bright band events. *Quart. J. Roy. Meteor. Soc.,* **124,** 2417–2434.

Vignal, B., and W. F. Krajewski, 2001: Large-scale evaluation of two methods to correct range-dependent error for WSR-88D rainfall estimates. *J. Hydrometeor.,* **2,** 490–504.

——, H. Andrieu, and J. D. Creutin, 1999: Identification of vertical profiles of reflectivity from volume scan radar data. *J. Appl. Meteor.,* **38,** 1214–1228.

——, G. Galli, J. Joss, and U. Germann, 2000: Three methods to determine profiles of reflectivity from volumetric radar data to correct precipitation estimates. *J. Appl. Meteor.,* **39,** 1715–1726.

Waldvogel, A., 1974: The N_0 jump of raindrop spectra. *J. Atmos. Sci.,* **31,** 1067–1078.

Zawadzki, I., W. Szyrmer, C. Bell, and F. Fabry, 2005: Modeling of the melting layer. Part III: The density effect. *J. Atmos. Sci.,* **62,** 3705–3723.